



# Ultrasound Imaging and Antithrombotic Effects of PLA-Combined Fe<sub>3</sub>O<sub>4</sub>-GO-ASA Multifunctional Nanobubbles

Jie Zhang<sup>1</sup>, Zheng Liu<sup>1</sup>, Cunyi Chang<sup>1</sup>, Ming Hu<sup>2</sup>, Yang Teng<sup>1</sup>, Jinjing Li<sup>1</sup>, Xiangyu Zhang<sup>1</sup> and Yanxia Chi<sup>3\*</sup>

<sup>1</sup> School of Pharmacy, Jiamusi University, Jiamusi, China, <sup>2</sup> School of Material Science and Engineering, Jiamusi University, Jiamusi, China, <sup>3</sup> School of Stomatology, Jiamusi University, Jiamusi, China

## OPEN ACCESS

### Edited by:

Francesco Rundo,  
STMicroelectronics, Italy

### Reviewed by:

Puja Panwar Hazari,  
Institute of Nuclear Medicine & Allied  
Sciences (DRDO), India  
Monica Argenziano,  
University of Turin, Italy

### \*Correspondence:

Yanxia Chi  
yanxiachi123@163.com

### Specialty section:

This article was submitted to  
Nuclear Medicine,  
a section of the journal  
Frontiers in Medicine

**Received:** 26 June 2020

**Accepted:** 30 March 2021

**Published:** 04 May 2021

### Citation:

Zhang J, Liu Z, Chang C, Hu M,  
Teng Y, Li J, Zhang X and Chi Y (2021)  
Ultrasound Imaging and  
Antithrombotic Effects of  
PLA-Combined Fe<sub>3</sub>O<sub>4</sub>-GO-ASA  
Multifunctional Nanobubbles.  
*Front. Med.* 8:576422.  
doi: 10.3389/fmed.2021.576422

PLA-combined ferromagnetic oxide-graphene oxide-aspirin (Fe<sub>3</sub>O<sub>4</sub>-GO-ASA) multifunctional nanobubbles were prepared using the double emulsion-solvent evaporation method. The obtained composite nanobubbles had a regular spherical shape, Zeta potential of  $(-36.5 \pm 10.0)$  mV, and particle size distribution range of 200–700 nm. The experimental results showed that PLA-combined Fe<sub>3</sub>O<sub>4</sub>-GO-ASA nanobubbles could effectively improve the antithrombin parameters of PT, TT, APTT, and INR, and significantly inhibit thrombosis when the composite nanobubbles with a concentration of 80 mg·mL<sup>-1</sup> interacted with the rabbit blood. The prepared composite nanobubbles could reach a significant ultrasonic imaging effect and good magnetic targeting under the magnetic field when the nanobubbles' concentration was only 60 mg·mL<sup>-1</sup>.

**Keywords:** graphene oxide, multifunctional nanobubbles, magnetic target, thrombosis, nanobubbles

## INTRODUCTION

At present, ultrasound contrast agents with the functions of targeted diagnosis, interventional therapy, and molecular imaging have become a popular research focus (1). The multifunctional ultrasonic contrast agent nanobubbles can not only improve the contrast and clarity of ultrasound images, but can also have other auxiliary effects by combining with other biomedical nanomaterials such as magnetic nanoparticles, drugs, and genes (2–4).

Timely diagnosis and treatment of thrombotic diseases are important for the prognosis and outcome of treatment. At present, the commonly targeted thrombolytic nanoparticles can be roughly divided into three types (5): magnetic nanoparticles loaded with the thrombolytic drugs (6, 7), a polylactic acid polymer material with the thrombolytic drugs (8, 9) and liposomes with thrombolytic drugs (10, 11). Ultrasonic imaging, as a medical diagnostic technology, has advantages such as being non-invasive, having low adverse reactions, and no radiation, as well as a convenient operation and real-time imaging, which means it shows great potential in the diagnosis of thrombotic diseases (12, 13). Ultrasonic imaging can not only be used to detect thrombosis symptoms, but also to dissolve blood clots (14). Studies have shown that ultrasound imaging can effectively dissolve the thrombus of the coronary arteries, cerebral aorta, and peripheral arteries, which results from the mechanical and cavitation effect during the ultrasound (15, 16). Platelet is the central link in thrombosis and plays a key role in thrombosis, particularly in arterial and microvascular thrombosis (17, 18). Aspirin (ASA) is one of the most widely used antiplatelet drugs

and is commonly used for the primary and secondary prevention and treatment of thrombocytosis or thrombosis.

Graphene oxide (GO) has good water solubility and biocompatibility (19, 20) due to the plentiful oxygen functional groups (such as -OH and -COOH) on its surface. GO can also load drugs with the benzene ring structure through the  $\pi$ - $\pi$  conjugation effect. These properties have made GO the focus in a wide range of research, such as in biosensor, bone material, targeted deliver medication, and other biomedical fields (21). As a kind of magnetic substance, nano-iron tetroxide ( $\text{Fe}_3\text{O}_4$ ) particle has various applications in magnetic targeting delivery systems. This is due to the fact that  $\text{Fe}_3\text{O}_4$  particle is non-toxic to cells, has good biocompatibility and excellent magnetic properties, and can be excreted from the body through degradation (22). Magnetic GO is also used in many applications; GO modified with  $\text{Fe}_3\text{O}_4$  nanoparticles was used for the nanocarrier of doxorubicin, which increased the targeted release effect of drugs (23). The magnetic GO functionalized with PEG could be used for localized photothermal ablation *in vitro* for cancer cells (24). In addition, magnetic GO is widely used for magnetic resonance imaging, molecular imaging probing, and other tasks.

In this study, GO was used as the carrier.  $\text{Fe}_3\text{O}_4$  nanoparticles as the magnetic targeting factor grew on its surface *in-situ*, and the GO- $\text{Fe}_3\text{O}_4$  magnetic targeting complex was obtained. Then acetyl salicylic acid (ASA) was loaded on the surface of GO- $\text{Fe}_3\text{O}_4$  complex by  $\pi$ - $\pi$  function. A PLA complexed with  $\text{Fe}_3\text{O}_4$ -GO-ASA multifunctional nanobubble was designed and prepared, and this composite nanobubble could perform magnetically targeted ultrasonic imaging on the thrombus site and simultaneously inhibit the thrombosis formation caused by platelet aggregation. This study hoped to provide a new avenue for the research and development of an ultrasonic contrast agent in the thrombosis field.

## MATERIALS AND METHODS

### Materials

$\text{FeCl}_2$  and  $\text{FeCl}_3$  was obtained from Beichen Founder Reagent Factory, Tianjin, China. Acetylsalicylic acid was obtained from ASA, McLean Co., Ltd., Shanghai, China and polylactic acid was supplied by PLA, Kemio Chemical Reagent Co., Ltd., Tianjin, China. Polyethylene glycol (PEG), polyvinyl alcohol (PVA), methylene chloride, isopropanol, and anhydrous ethanol were obtained from Kaitong Chemical Reagent Co., Ltd., Tianjin, China, while New Zealand white rabbits and Kunming mice were provided by Jiamusi University Animal Experimental Center, Heilongjiang, China.

### Characterization

The average particle size and Zeta potential of the nanobubbles were measured by laser particle size tester (DLS). The loading rate of ASA in  $\text{Fe}_3\text{O}_4$ -GO-ASA complex was determined by UV-visible spectrophotometer (UV-vis), and the chemical composition of GO-ASA complex was determined by Fourier transform infrared spectroscopy (FT-IR). Scanning electron microscope (SEM) and Transmission electron microscopy (TEM) were used to observe the microscopic morphology

of PLA-combined  $\text{Fe}_3\text{O}_4$ -GO-ASA nanobubbles. The magnetic properties of  $\text{Fe}_3\text{O}_4$  nanoparticles,  $\text{Fe}_3\text{O}_4$ -GO complex, and PLA-combined  $\text{Fe}_3\text{O}_4$ -GO-ASA nanobubbles were determined by sample vibration magnetometer (VSM).

### Preparation of $\text{Fe}_3\text{O}_4$ -GO Complex

First, GO was prepared by an improved Hummers method (25).  $\text{Fe}_3\text{O}_4$ -GO complex was synthesized by *in-situ* growth method.  $\text{FeCl}_2$  of 0.23g and  $\text{FeCl}_3$  of 0.47g were dissolved in the dual-distilled water and placed in a round-bottomed flask. Polyethylene glycol (PEG,  $M_w = 1,000$ ) was added under stirring at 60°C. GO of 0.15g was dispersed in dual-distilled water and added into the above system. Meanwhile, the pH of this system was kept at 10–11 by the drop wise addition of NaOH solution and the reaction was maintained for 20 min. Then, the system was heated to 80°C and aged for 30 min. The resulting precipitation was repeatedly washed with the dual-distilled water to neutral, and  $\text{Fe}_3\text{O}_4$ -GO complex was obtained by vacuum freeze drying.

### Preparation of $\text{Fe}_3\text{O}_4$ -GO-ASA Complex

Of the  $\text{Fe}_3\text{O}_4$ -GO complex, 0.1 g was added to an appropriate amount of anhydrous ethanol for ultrasonic dispersion. Then ASA of 0.2 g was added into the dispersion system of  $\text{Fe}_3\text{O}_4$ -GO complex and this mixture system was stirred at 25°C for 2 h. Finally, the precipitation was repeatedly washed by the anhydrous ethanol and treated by vacuum freeze drying to obtain the  $\text{Fe}_3\text{O}_4$ -GO-ASA complex.

### Preparation of PLA-Combined $\text{Fe}_3\text{O}_4$ -GO-ASA Nanobubbles

PLA-combined  $\text{Fe}_3\text{O}_4$ -GO-ASA nanobubbles were prepared by the double emulsion-solvent evaporation method. PLA of 0.6 g was dissolved in the methylene dichloride and a certain amount of the dispersion liquid of  $\text{Fe}_3\text{O}_4$ -GO-ASA complex was added, with ultrasonic emulsification under nitrogen for 5 min. The primary emulsion of W/O was obtained this way. Then primary emulsion of W/O was added into the aqueous solution of polyvinylalcohol (PVA) and ultrasonic emulsification was again performed to get the multiple emulsion of W/O/W. Multiple emulsion of W/O/W was added into aqueous solution of isopropyl alcohol. The mixed system was stirred for 6 h and washed with the centrifugal machine three times, and the obtained supernatant was retained for later use. The obtained precipitation was freeze-dried to obtain PLA-combined  $\text{Fe}_3\text{O}_4$ -GO-ASA nanobubbles.

### Ultrasonic Imaging Experiment

Of the four New Zealand rabbits, one was injected with 2 mL physiological saline, and the other three were, respectively, injected with 2 mL PLA-combined  $\text{Fe}_3\text{O}_4$ -GO-ASA nanobubbles with concentrations of 20, 60, and 100 mg·mL<sup>-1</sup> physiological saline solution through the auricular vein. The abdominal cavity was opened at the lower abdomen cut of the rabbit xiphoid and the abdominal aorta shell was stripped off. After the abdominal aorta was exposed, this segment of blood vessel was applied with the filter paper that was soaked in  $\text{FeCl}_3$  solution. After 15 min, the filter paper was removed and the abdomen was

stitched. The composite nanobubbles suspension liquid was injected through the rabbit ear vein and the ultrasonic test (3.5 MHz) on the abdominal aorta was carried out with and without external magnetic field. This present study received protocol approval from the university's Institutional Animal Care and Use Committee (IACUC).

### Anti-thrombotic Experiment *in vitro*

A certain amount of PLA-combined  $\text{Fe}_3\text{O}_4$ -GO-ASA nanobubbles were ultrasonically broken in normal saline for 2 h. The broken solution was, respectively, diluted to 20, 40, 60, 80, and 100  $\text{mg}\cdot\text{mL}^{-1}$ . Some blood was collected from the ear vein of rabbit. 0.1 mL broken solution with the different concentrations interacted with 2 mL of rabbit blood. Then, the obtained blood sample was added into a small test tube containing No.1 surgical line, and the test tube was kept in a water bath of  $37^\circ\text{C}$  for 1.5 h. Finally, the formed blood clot was taken, and the wet weight and dry weight were weighed and compared (26).

Another broken solution with different concentrations interacted with 2 mL of rabbit blood for 1 h, and PT, TT, APTT, and INR values of blood samples were, respectively, measured by semi-automatic blood coagulation analyzer (URJT-600, Uritest, Guilin, China).

### Biocompatibility

Kunming mice of 23~25 g were divided into five groups, with three mice in each group. Mice were prostrated and fixed on the experimental table. 0.2 mL of PLA-combined  $\text{Fe}_3\text{O}_4$ -GO-ASA nanobubbles ( $150\text{ mg}\cdot\text{mL}^{-1}$ ) were subcutaneously injected into the back of mice. The control group was injected with 0.2 mL of normal saline. Mice in the control group were sacrificed at 1 day and those of the composite nanobubbles group were, respectively, sacrificed at 1, 3, 9, and 21 days after injection, and the local tissue of the injection site was observed. At the same time, the muscle at the injection site was taken and fixed in 10% formalin solution for preservation. The samples were conventionally dehydrated and embedded with the paraffin. After HE staining, samples were observed with the light microscope (27).

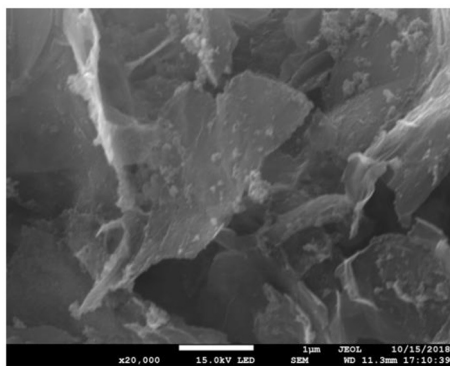


FIGURE 1 | SEM of  $\text{Fe}_3\text{O}_4$ -GO complex.

## RESULTS

Figure 1 shows SEM of  $\text{Fe}_3\text{O}_4$ -GO complex. It can be seen from Figure 1 that there were some nanoparticles on GO nanosheet, which was due to the deposition of  $\text{Fe}_3\text{O}_4$  nanoparticles on the GO by the *in-situ* growth method. Figure 2 shows the infrared spectra of ASA, GO, and GO-ASA complex. In Figure 2a, the absorption peak near  $3,000\text{ cm}^{-1}$  was the  $-\text{COOH}$  characteristic peak, the absorption peak near  $1,600\text{ cm}^{-1}$  was the stretching vibration peak of benzene ring skeleton, the absorption peaks at  $1,224$  and  $1,110\text{ cm}^{-1}$  were caused by C-O stretching vibration, and the absorption peak at  $750\text{ cm}^{-1}$  was attributed to the vicinal substitution of benzene ring. These peaks were the most obvious characteristics of aspirin. It can be seen from Figure 2b that the absorption peak near  $3,430\text{ cm}^{-1}$  was attributed to the stretching vibration peak of  $-\text{OH}$  in  $-\text{COOH}$ , the absorption peak at  $1,643\text{ cm}^{-1}$  was caused by the bending vibration of  $-\text{COOH}$  on the edge of GO, and the absorption peak near  $1,310\text{ cm}^{-1}$  was the C-O stretching vibration peak. The presence of these oxygen-containing groups indicated that graphite was oxidized. From Figure 2c, the absorption peak at  $3,430$ ,  $1,643$ , and  $1,310\text{ cm}^{-1}$  belonged to the GO characteristic peak. The absorption peak at  $1,110\text{ cm}^{-1}$  was the stretching vibration peak of C-O in ASA. The absorption peak of benzene ring appeared near  $740\text{ cm}^{-1}$  and moved toward the low wave number, which was caused by the formed  $\pi$ -hydrogen bond between ASA and GO (28). As a result, ASA was loaded on GO by  $\pi$ - $\pi$  conjugation in the study.

Figures 3–5, respectively, show the SEM, particle size distribution, and Zeta potential of PLA-combined  $\text{Fe}_3\text{O}_4$ -GO-ASA nanobubbles. It can be seen from Figures 3, 4 that the obtained composite nanobubbles had a smooth surface, clear boundary, and uniform size, and the particle size of the nanobubbles was 200–700 nm, which met the clinical requirements of ultrasound contrast agent. Among them, the composite nanobubbles presented the irregular spheres shown

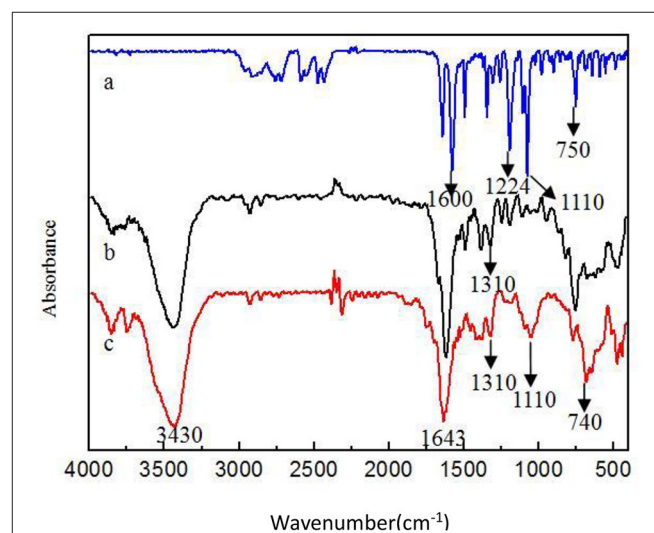
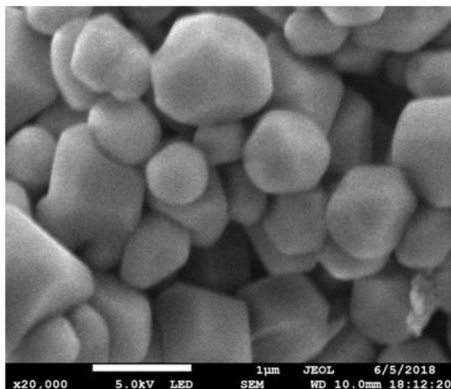
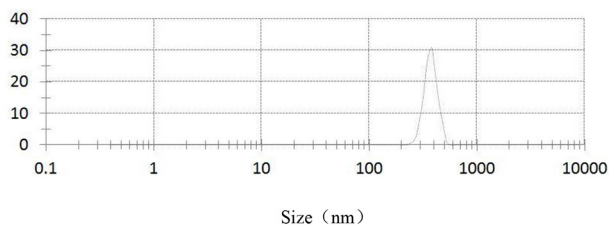


FIGURE 2 | Infrared spectra of different samples (a) ASA (b) GO (c) GO-ASA.



**FIGURE 3** | SEM of PLA combined  $\text{Fe}_3\text{O}_4$ -GO-ASA nanobubbles.



**FIGURE 4** | Particle size distribution of PLA combined  $\text{Fe}_3\text{O}_4$ -GO-ASA nanobubbles.

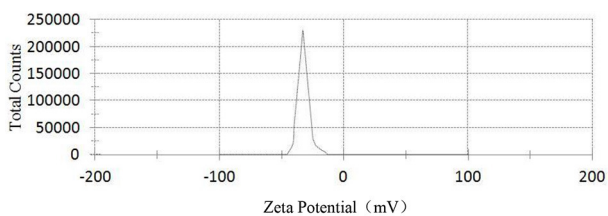


**FIGURE 5** | Zeta potential of PLA combined  $\text{Fe}_3\text{O}_4$ -GO-ASA nanobubbles.

in **Figure 3**, resulting from the freeze drying process of the composite nanobubbles. According to **Figure 5**, Zeta potential of the composite nanobubbles was  $(-36.5 \pm 10.0)$  mV, which proved that aqueous solution of the composite nanobubbles had good dispersion stability.

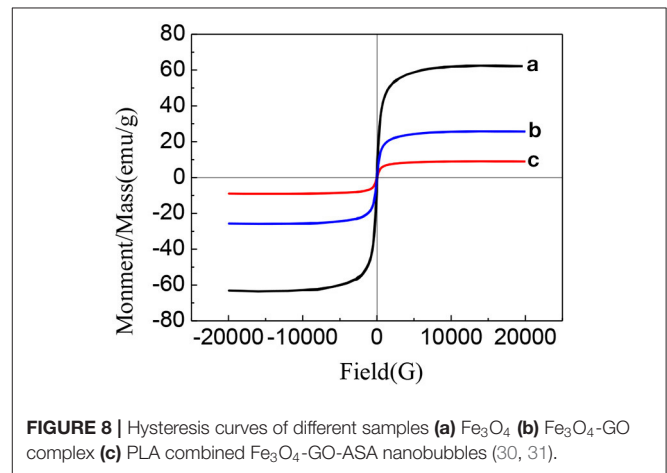
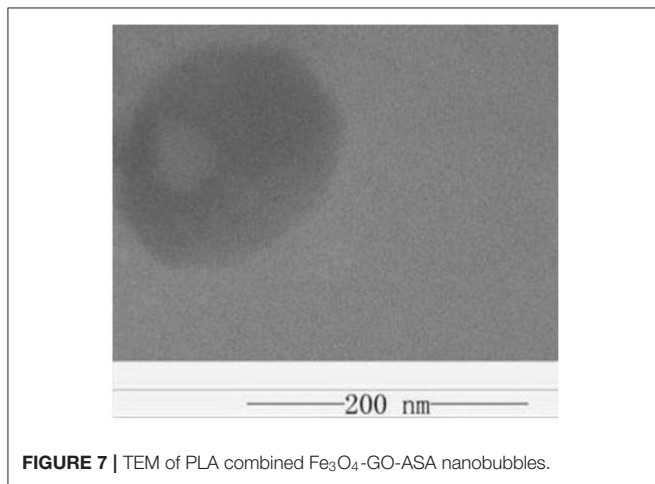
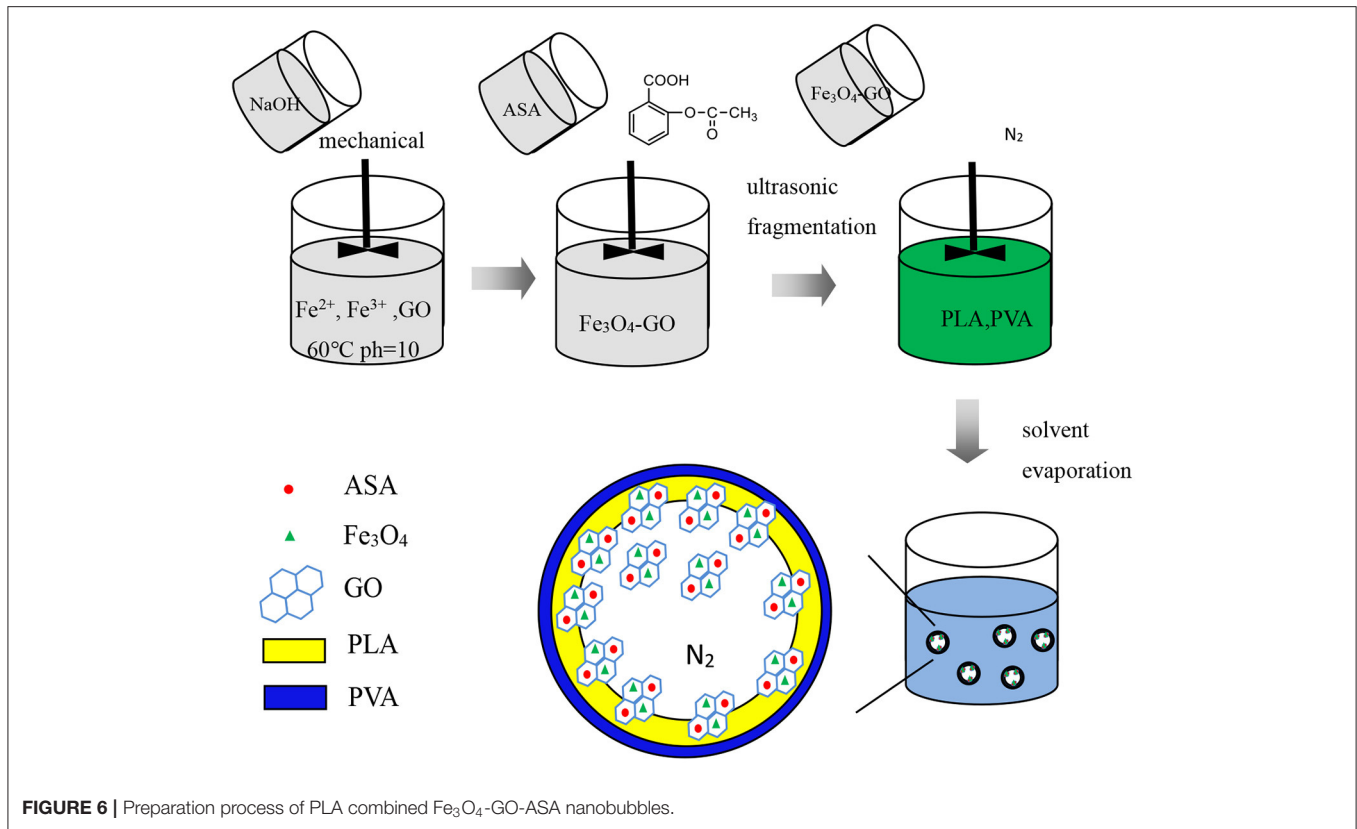
**Figures 6, 7**, respectively, show the preparation process and TEM of PLA-combined  $\text{Fe}_3\text{O}_4$ -GO-ASA nanobubbles. In the preparation process,  $\text{Fe}_3\text{O}_4$  was firstly grown on the GO surface by an *in-situ* growth method and ASA was loaded on  $\text{Fe}_3\text{O}_4$ -GO by  $\pi$ - $\pi$  conjugation effect to obtain  $\text{Fe}_3\text{O}_4$ -GO-ASA complex. Then,  $\text{Fe}_3\text{O}_4$ -GO-ASA complex was encapsulated in PLA nanobubbles by double emulsion-solvent evaporation method. During the first ultrasonic emulsification, PLA solution was destroyed into some small droplet wrapping  $\text{Fe}_3\text{O}_4$ -GO-ASA complex in the inner water phase. Due to the continuous  $\text{N}_2$  that was imported in the process of ultrasonic breaking, small bubbles

also contained  $\text{N}_2$ . At this moment, the obtained W/O phase was transferred to the PVA solution and evenly stirred, and the second ultrasonic emulsification was performed. As a result, PVA would coat on the surface of PLA nanobubbles by hydrogen bonding to form a hard shell (29). After the vacuum freeze drying, the water in the nanobubbles disappeared, and  $\text{Fe}_3\text{O}_4$ -GO-ASA complex would gather at the inner side of the nanobubble or embed in the film of the nanobubble due to the surface tension. As shown in **Figure 7**, the film and inner side of the nanobubble presented a black shadow.

**Figure 8** shows the hysteresis curves of  $\text{Fe}_3\text{O}_4$ ,  $\text{Fe}_3\text{O}_4$ -GO complex, and PLA-combined  $\text{Fe}_3\text{O}_4$ -GO-ASA nanobubbles (30, 31). As can be seen from **Figure 8**, the hysteresis curves of  $\text{Fe}_3\text{O}_4$ ,  $\text{Fe}_3\text{O}_4$ -GO complex, and PLA-combined  $\text{Fe}_3\text{O}_4$ -GO-ASA nanobubbles presented a similar pattern, meaning that their magnetic behaviors were similar. There was no coercive field nor residual magnetism at the zero point, which indicated that three samples had paramagnetic characteristics and could gather under external magnetic field conditions (32). In addition, the specific saturation magnetization intensity of  $\text{Fe}_3\text{O}_4$ ,  $\text{Fe}_3\text{O}_4$ -GO complex and PLA-combined  $\text{Fe}_3\text{O}_4$ -GO-ASA nanobubbles decreased orderly; this was because the  $\text{Fe}_3\text{O}_4$  content in the three samples of the same mass decreased in sequence, indicating that the magnetism of the  $\text{Fe}_3\text{O}_4$ -GO complex and PLA-combined  $\text{Fe}_3\text{O}_4$ -GO-ASA nanobubbles were derived from  $\text{Fe}_3\text{O}_4$ .

**Figure 9** is the ultrasonic imaging of rabbit abdominal aorta of PLA-combined  $\text{Fe}_3\text{O}_4$ -GO-ASA nanobubbles with different concentrations. As can be seen from **Figure 9A**, when PLA-combined  $\text{Fe}_3\text{O}_4$ -GO-ASA nanobubbles were not injected, the ultrasonic imaging of rabbit abdominal aorta was dark and very fuzzy. When the concentration of PLA-combined  $\text{Fe}_3\text{O}_4$ -GO-ASA nanobubbles were  $20 \text{ mg}\cdot\text{mL}^{-1}$  (**Figure 9B**), the ultrasonic signal was enhanced, and the contrast and identification of the image was significantly improved. When the concentration of PLA-combined  $\text{Fe}_3\text{O}_4$ -GO-ASA nanobubbles was  $>60 \text{ mg}\cdot\text{mL}^{-1}$  (**Figures 9C,D**), the effect of ultrasound imaging for the abdominal aorta was significantly improved, while the contrast of the image did not significantly change with the increase of PLA-combined  $\text{Fe}_3\text{O}_4$ -GO-ASA nanobubbles concentration. As a result, the ultrasonic effect had reached the requirements of ultrasound imaging when the concentration of PLA-combined  $\text{Fe}_3\text{O}_4$ -GO-ASA nanobubbles was  $60 \text{ mg}\cdot\text{mL}^{-1}$ .

PLA-combined  $\text{Fe}_3\text{O}_4$ -GO-ASA nanobubbles were injected into the model rabbit with abdominal aortic thrombus, and ultrasonic imaging photos of rabbit abdominal aorta with and without magnetic field are shown in **Figure 10**. From **Figure 10A**, a strong and distinct blue signal appeared in the right side of the thrombus, indicating the reflux blood presented at the thrombus obstruction site. At the same time, the composite nanobubbles were carried by blood and would flow throughout the body, and the ultrasonic signals could present in the tissues or organs where the composite nanobubbles passed through. As a result, a weak and large dark blue signal also appeared below the abdominal aorta of the rabbit. It can be seen from **Figure 10B** that when the magnetic field was added in the abdominal aorta region, the intensity of ultrasonic



signal in this region was significantly enhanced, while the signal intensity in other regions was significantly weakened, indicating that PLA-combined  $\text{Fe}_3\text{O}_4$ -GO-ASA nanobubbles could effectively enrich in the magnetic field region. Thus, the obtained PLA-combined  $\text{Fe}_3\text{O}_4$ -GO-ASA nanobubbles had a magnetic targeting effect under the action of an external magnetic field, which could significantly enhance the image clarity of the observed site without increasing the dosage of the composite nanobubbles.

**Table 1** shows the wet weight and dry weight of the obtained coagulated blood clot due to the interaction between PLA-combined  $\text{Fe}_3\text{O}_4$ -GO-ASA nanobubbles with different concentrations and blood samples. It can be seen from **Table 1** that the wet weight of the normal saline control group was  $95.10 \pm 0.22$  mg, while the wet weights for the composite nanobubbles with the concentrations of 20, 40, 60, 80, and 100  $\text{mg}\cdot\text{mL}^{-1}$  were, respectively,  $87.27 \pm 0.16$  mg,  $75.73 \pm 0.47$  mg,  $56.57 \pm 0.32$  mg,  $44.80 \pm 0.16$  mg, and  $36.03 \pm 0.22$  mg, showing the

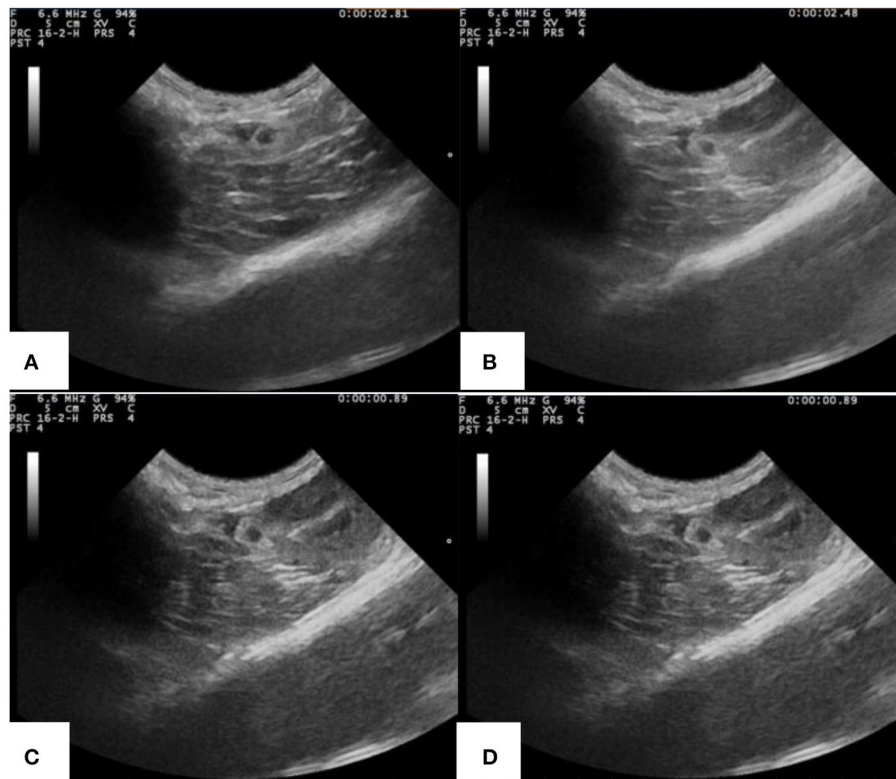


**FIGURE 9** | Ultrasonic imaging of rabbit abdominal aorta of rabbits injected with PLA combined  $\text{Fe}_3\text{O}_4$ -GO-ASA nanobubbles of the different concentrations (A)  $0 \text{ mg}\cdot\text{mL}^{-1}$  (B)  $20 \text{ mg}\cdot\text{mL}^{-1}$  (C)  $60 \text{ mg}\cdot\text{mL}^{-1}$  (D)  $100 \text{ mg}\cdot\text{mL}^{-1}$ .

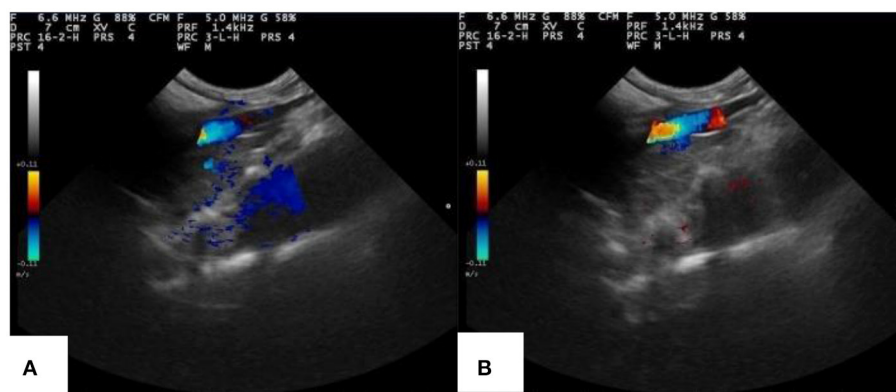


**FIGURE 10** | Ultrasonic imaging of rabbit abdominal aorta of rabbits injected with PLA combined  $\text{Fe}_3\text{O}_4$ -GO-ASA nanobubbles (A) without the magnetic field (B) with the additional magnetic field in the thrombus area.

composite nanobubbles were very significantly different from the control group ( $P < 0.01$ ). The dry weight of the normal saline control group was  $52.03 \pm 0.35 \text{ mg}$  and the dry weight of the composite nanobubble with the concentration of  $20 \text{ mg}\cdot\text{mL}^{-1}$  was  $50.17 \pm 0.35 \text{ mg}$ ; it was significantly different from the control group ( $0.01 < P < 0.05$ ). When the composite nanobubble concentration was 40, 60, 80, and  $100 \text{ mg}\cdot\text{mL}^{-1}$ , their dry weights were, respectively,  $44.83 \pm 0.36 \text{ mg}$ ,  $36.67 \pm 0.50 \text{ mg}$ ,  $33.03 \pm$

$0.75 \text{ mg}$ , and  $27.57 \pm 0.60 \text{ mg}$  and had very significant differences in comparison with the control group ( $P < 0.01$ ). We could see that the wet weight and dry weight of clots significantly decreased with the concentration increase of the composite nanobubbles.

This was because the ASA content in the composite nanobubbles increased with the increase of the composite nanobubbles concentration, and ASA had an inhibitory effect on the thrombosis (33). The antithrombotic effect of ASA is mainly

realized by inhibiting the activity of the platelet cyclooxygenase and preventing the synthesis and release of prostaglandins and thromboxane (34). Moreover, we could conclude from **Table 1** that the ratio of wet weight and dry weight of clots decreased with the increase of the composite nanobubbles concentration. For the formation of thrombus, the ratio of wet weight and dry weight ratio is smaller and the dissociation of thrombus factor in the blood is stronger, thus the speed of thrombosis caused by factors becomes slow. The ratio of wet weight and dry weight is lower, indicating that the risk of thrombosis is smaller. It can be seen that the anti-thrombotic ability of PLA-combined

$\text{Fe}_3\text{O}_4$ -GO-ASA nanobubbles increased with the increase of its concentration.

**Table 2** shows the changes of the coagulated blood parameters due to the interaction between PLA-combined  $\text{Fe}_3\text{O}_4$ -GO-ASA nanobubbles of different concentrations and blood samples. As can be seen from **Table 2**, the values of PT, TT, APTT, and INR in blood samples showed an increasing trend with the increase of the composite nanobubbles concentration. Specifically, APTT value significantly increased when the composite nanobubbles concentration was  $20 \text{ mg}\cdot\text{mL}^{-1}$ , PT and TT values significantly increased at the concentration of  $40 \text{ mg}\cdot\text{mL}^{-1}$ , and INR value significantly increased at the concentration of  $80 \text{ mg}\cdot\text{mL}^{-1}$ . It can be seen that when the concentration of the composite nanobubbles was above  $80 \text{ mg}\cdot\text{mL}^{-1}$ , they could effectively promote the synthesis of cAMP in platelet and interdict the platelet membrane glycoproteins receptors, which reduced the concentrations of thromboxane A and phosphodiesterase in plasma and eventually inhibited the formation process of thrombosis. So, PLA-combined  $\text{Fe}_3\text{O}_4$ -GO-ASA nanobubbles could effectively inhibit thrombosis and achieve the purpose of adjuvant therapy.

**Figure 11** is the HE staining pictures of mouse muscle after the subcutaneous injection of normal saline and PLA-combined  $\text{Fe}_3\text{O}_4$ -GO-ASA nanobubbles at different times. As shown in **Figure 11A**, mouse muscle tissue had an intact structure and the histopathological change was not observed for the normal saline group. For PLA-combined  $\text{Fe}_3\text{O}_4$ -GO-ASA nanobubbles, the injection site of 1 day formed a cyst by the experimental observation, while the cyst had a thin wall and it contained the nanobubbles injection solution and interstitial fluid. As shown in **Figure 11B**, compared with the saline group, there was a slight inflammatory cell infiltration at the injection site. After PLA-combined  $\text{Fe}_3\text{O}_4$ -GO-ASA nanobubbles were injected for 3 days, the formed cyst at the

**TABLE 1** | Wet weight and dry weight of the coagulated blood clot.

Concentration ( $\text{mg}\cdot\text{mL}^{-1}$ )	Wet weight (mg)	Dry weight (mg)
0	$95.10 \pm 0.22$	$52.03 \pm 0.35$
20	$87.27 \pm 0.16^{**}$	$50.17 \pm 0.35^*$
40	$75.73 \pm 0.47^{**}$	$44.83 \pm 0.36^{**}$
60	$56.57 \pm 0.32^{**}$	$36.67 \pm 0.50^{**}$
80	$44.80 \pm 0.16^{**}$	$33.03 \pm 0.75^{**}$
100	$36.03 \pm 0.22^{**}$	$27.57 \pm 0.60^{**}$

\* $P < 0.05$ , \*\* $P < 0.01$ .

**TABLE 2** | Effects of PLA combined  $\text{Fe}_3\text{O}_4$ -GO-ASA nanobubbles with the different concentrations on the coagulation blood parameters.

Concentration ( $\text{mg}\cdot\text{mL}^{-1}$ )	PT(s)	TT(s)	APTT(s)	INR(s)
0	13.2	14.0	29.6	1.09
10	13.5	14.5	29.7	1.11
20	13.7	15.7	30.1	1.16
40	15.3	16.4	30.9	1.23
80	17.2	18.0	32.8	1.45
160	18.8	20.1	33.6	1.56

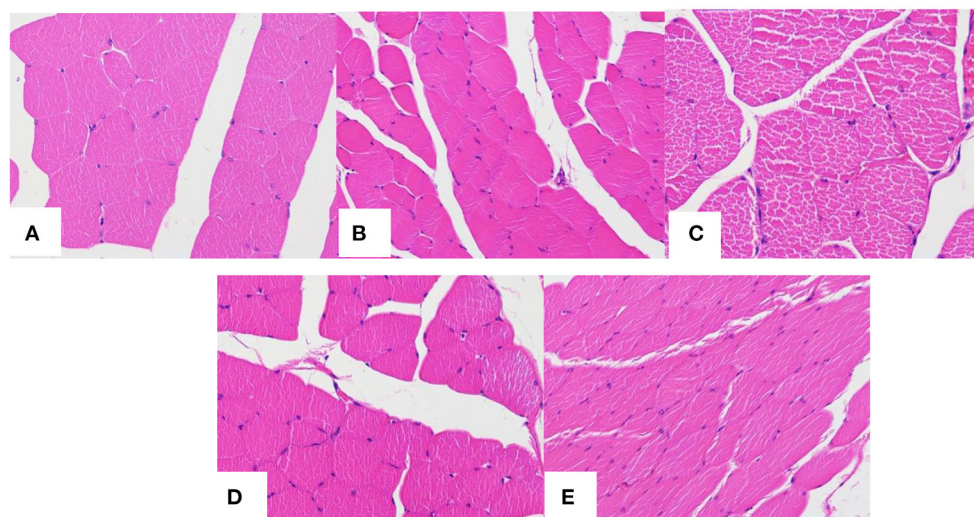


**FIGURE 11** | HE staining pictures of mouse muscle after the subcutaneous injection of saline at 1 day (A) and the composite nanobubbles at 1 day (B), 3 days (C), 9 days (D), and 21 days (E).

injection site significantly reduced, and the inflammatory cell infiltration was weakened as shown in **Figure 11C**, however, the infiltration phenomenon did not disappear because the degradation products of the composite nanobubbles were not eliminated or absorbed in a timely manner. At 9 days after injection, the local cyst basically disappeared, and the inflammatory cell infiltration significantly reduced (**Figure 11D**). At 21 days after injection, the inflammatory cell infiltration disappeared (**Figure 11E**), and there was no obvious change in the deep muscle tissue. Therefore, the injection of PLA-combined Fe<sub>3</sub>O<sub>4</sub>-GO-ASA nanobubbles only caused a slight inflammatory response, and the accumulation of tissue penetrating fluid or obvious proliferation of vascular or fibers was not observed, indicating that PLA-combined Fe<sub>3</sub>O<sub>4</sub>-GO-ASA nanobubbles have good biocompatibility.

## CONCLUSIONS

In this study, the nanobubbles were prepared in three steps. Firstly, Fe<sub>3</sub>O<sub>4</sub> nanoparticles were deposited on GO using an *in-situ* growth method. Then, ASA was adsorbed on the Fe<sub>3</sub>O<sub>4</sub>-GO composite through  $\pi$ - $\pi$  effect. Finally, the newly formed Fe<sub>3</sub>O<sub>4</sub>-GO-ASA composite was combined into the PLA nanobubbles by the double emulsion-solvent evaporation method.

The obtained PLA-combined Fe<sub>3</sub>O<sub>4</sub>-GO-ASA nanobubbles can inhibit thrombosis and effectively enrich the target area under the action of a magnetic field to achieve the targeted imaging effect. Moreover, if the ultrasonic power was increased, the composite nanobubbles could be broken and the controlled drug release achieved, indicating that PLA-combined Fe<sub>3</sub>O<sub>4</sub>-GO-ASA nanobubbles could realize the dual functions of targeted drug delivery and controlled release. However, the antithrombotic performance of PLA-combined Fe<sub>3</sub>O<sub>4</sub>-GO-ASA nanobubbles *in vivo* will need further study. This study lays a foundation for the development and application of magnetic targeted ultrasound contrast agents.

## REFERENCES

- Liu R, Tang J, Xu Y, Dai Z. BRET-FRET nanobubbles for bioluminescence/ultrasound dual-modal imaging of Inflammation *in vivo*, bioluminescence imaging of inflammation *in vivo* based on bioluminescence and fluorescence resonance energy transfer using nanobubbles ultrasound contrast agent. *ACS Nano*. (2019) 13:5124–32. doi: 10.1021/acsnano.8b08359
- de Leon A, Perera R, Nittayacharn P, Cooley M, Jung O, Exner AA. Ultrasound contrast agents and delivery systems in cancer detection and therapy. *Adv Cancer Res*. (2018) 139:57–84. doi: 10.1016/bs.acr.2018.04.002
- Koczera P, Appold L, Shi Y, Liu M, Dasgupta A, Pathak V, et al. PBCA-based polymeric microbubbles for molecular imaging and drug delivery. *J Control Release*. (2017) 259:128–35. doi: 10.1016/j.jconrel.2017.03.006
- Martin KH, Dayton PA. Current status and prospects for microbubbles in ultrasound theranostics. *Wiley Interdiscip Rev Nanomed Nanobiotechnol*. (2013) 5:329–45. doi: 10.1002/wnan.1219
- Zhou J, Guo DJ. Research progress of targeted thrombolysis in drug delivery system. *Chongqing Med*. (2014) 43:617–20. doi: 10.3969/j.issn.1671-8348.2014.05.042
- Chen JP, Yang PC, Ma YH, Wu T. Characterization of chitosan magnetic nanoparticles for in situ delivery of tissue plasminogen activator. *Carbohydr Polym*. (2011) 84:364–72. doi: 10.1016/j.carbpol.2010.11.052
- Ma YH, Wu SY, Wu T, Chang YJ, Hua MY, Chen JP. Magnetically targeted thrombolysis with recombinant tissue plasminogen activator bound to polyacrylic acid-coated nanoparticles. *Biomaterials*. (2009) 30:3343–51. doi: 10.1016/j.biomaterials.2009.02.034
- Zhou J. *Construction and Characterization of Multifunctional MR Molecular Probe Carrying rtPA Targeting Thrombus [D]*. Chongqing: Chongqing Medical University (2014). doi: 10.7666/d.Y2690646
- Zhong YX. *Phase Variant Multimodal Nanoparticle Thrombosis Imaging and Thrombolysis of Targeted Fibrin [D]*. Chongqing: Chongqing Medical University (2019).
- Hua X. *Preparation of Ultrasonic Contrast Agent Containing tPA and RGDs and Mechanism of Drug Release and Solubilization [D]*. Chongqing: Third Military Medical University (2007). doi: 10.7666/d.y1179627
- Laing ST, Moody MR, Kim H, Smulevitz B, Huang SL, Holland CK, et al. Thrombolytic efficacy of tissue plasminogen activator-loaded echogenic liposomes in a rabbit thrombus. *Thromb Res*. (2012) 130:629–35. doi: 10.1016/j.thromres.2011.11.010

## DATA AVAILABILITY STATEMENT

The original contributions presented in the study are included in the article/**Supplementary Material**, further inquiries can be directed to the corresponding author/s.

## ETHICS STATEMENT

The animal study was reviewed and approved by Ethics Committee of Jiamusi university Jiamusi university.

## AUTHOR CONTRIBUTIONS

JZ and YC are responsible for the design of experimental direction, arrangement of experimental methods, revision, and proofreading of this paper. ZL and CC were responsible for the implementation of the experiment and the preliminary writing of the paper. MH, YT, JL, and XZ were responsible for the evaluation of experimental design.

## FUNDING

This work was supported by National Natural Science Foundation of China (Nos. 51671096 and 81601616), Excellent innovation team based on the basic scientific research vocational cost for the provincial undergraduate universities in Heilongjiang (No. 2018-KYYWF-0914), Heilongjiang Health Department Project (2017-419), and Heilongjiang Education Department Project (2017-KYYWF-0601).

## SUPPLEMENTARY MATERIAL

The Supplementary Material for this article can be found online at: <https://www.frontiersin.org/articles/10.3389/fmed.2021.576422/full#supplementary-material>

12. Ebel H, Offhaus A, Wiora M, Roehl P, Schwenzky A, Weida A, et al. Impact of ultrasound contrast agent on the detection of thrombi during transoesophageal echocardiography. *Open Heart*. (2019) 6:e00124. doi: 10.1136/openhrt-2019-001024
13. Plachá D, Jampilek J. Graphenic materials for biomedical applications. *Nanomaterials*. (2019) 9:1–37. doi: 10.3390/nano9121758
14. Zhang B, Wang H. Progress in clinical application of ultrasonic thrombolysis. *Chin J Med Ultrasound*. (2019) 16:785–9. doi: 10.3877/cma.j.issn.1672-6448.2019.10.013
15. Chernysh IN, Everbach CE, Purohit PK, Weisel JW. Molecular mechanisms of the effect of ultrasound on the fibrinolysis of clots. *J Thromb Haemost*. (2015) 13:601–9. doi: 10.1111/jth.12857
16. Lee TH, Yeh JC, Tsai CH, Yang JT, Lou SL, Seak CJ, et al. Improved thrombolytic effect with focused ultrasound and neuroprotective agent against acute carotid artery thrombosis in rat. *Sci Rep*. (2017) 7:1638. doi: 10.1038/s41598-017-01769-2
17. Huang Y, Chen KJ, Yin HJ. Thrombus formation and prevention and treatment of traditional Chinese medicine. *Med. Rev*. (2010) 16:1410–3. doi: 10.3969/j.issn.1006-2084.2010.09.045s
18. Feng ZC. Chronic inflammation of the atherosclerotic vessel wall. *Chin. J. Cardiol*. (2005) 33:393–4. doi: 10.3760/j.issn:0253-3758.2005.05.001
19. Qiu ZC. *Graphene Oxide-Based Nanocomposite for Targeting Colorectal Cancer Therapy*. Wuxi: Jiangnan University (2020). doi: 10.27169/d.cnki.gwqgu.2020.000296
20. Hussien NA, Işiklan N, Türk M. Pectin-conjugated magnetic graphene oxide nanohybrid as a novel drug carrier for paclitaxel delivery. *Artif Cells Nanomed Biotechnol*. (2018) 46:264–73. doi: 10.1080/21691401.2017.1421211
21. Liu J, Xu F, Huang J, Xu J, Liu Y, Yao Y, et al. Low-intensity focused ultrasound (LIFU)-activated nanodroplets as a theranostic agent for noninvasive cancer molecular imaging and drug delivery. *Biomater Sci*. (2018) 6:2838–49. doi: 10.1039/C8BM00726H
22. Zhang F. *Preparation of Magnetic Go Based Non-covalent Modified Nanocomposites and Their Application in Drug Delivery*. Zhenjiang: Jiangsu University (2019). doi: 10.27170/d.cnki.gjsuu.2019.000049
23. Yang X, Zhang X, Ma Y, Huang Y, Wang Y, Chen Y. Superparamagnetic graphene oxide-Fe<sub>3</sub>O<sub>4</sub> nanoparticles hybrid for controlled targeted drug carriers. *J Materials Chem*. (2009) 19:2710–4. doi: 10.1039/b821416f
24. Shi S, Yang K, Hong H, Valdovinosd HF, Nayakc TR, Zhang Y, et al. Tumor vasculature targeting and imaging in living mice with reduced graphene oxide. *Biomaterials*. (2013) 34:3002–9. doi: 10.1016/j.biomaterials.2013.01.047
25. Ren L, Pan S, Li H, Li Y, He L, Zhang S, et al. Effects of aspirin-loaded graphene oxide coating of a titanium surface on proliferation and osteogenic differentiation of MC3T3-E1 cells. *Sci Rep*. (2018) 8:15143–56. doi: 10.1038/s41598-018-33353-7
26. Lei H, Hu Y, Li G. Magnetic poly(phenylene ethynylene) conjugated microporous polymer microspheres for bactericides enrichment and analysis by ultra-high performance liquid chromatography-tandem mass spectrometry. *Chromatogr A*. (2018) 1580:22–29. doi: 10.1016/j.chroma.2018.10.043
27. Otani K, Nishimura H, Kamiya A, Harada-Shiba M. Simplified preparation of  $\alpha v \beta 3$  integrin-targeted nanobubbles based on a clinically available ultrasound contrast agent: validation in a tumor-bearing mouse model. *Ultrasound Med Biol*. (2018) 44:1063–73. doi: 10.1016/j.ultrasmedbio.2018.01.017
28. Xu Y. *The Regulation of  $\pi$ -Conjugate Oligomer Aggregation Behavior by Hydrogen Bond and  $\pi$ - $\pi$  Synergy [D]*. Changchun: Jilin University (2009).
29. Abdal-Hay A, Hussein KH, Casettari L, Khalil KA, Hamdy AS. Fabrication of novel high performance ductile poly (lactic acid) nanofiber scaffold coated with poly(vinyl alcohol) for tissue engineering applications. *Mater Sci Eng C Mater Biol Appl*. (2016) 60:143–50. doi: 10.1016/j.msec.2015.11.024
30. Zhang J, Yang J, Zhang H, Hu M, Lia J, Zhanga X. New Span-PEG-composited Fe<sub>3</sub>O<sub>4</sub>-CNT as a multifunctional ultrasound contrast agent for inflammation and thrombotic niduses. *RSC Adv*. (2020) 10:38592–600. doi: 10.1039/D0RA05401A
31. Zhang J, Liu Z, Zhou S, Teng Y, Zhang X, Li J. Novel span-PEG multifunctional ultrasound contrast agent based on CNTs as a magnetic targeting factor and a drug carrier. *ACS Omega*. (2020) 5:31525–34. doi: 10.1021/acsomega.0c03325
32. Tang H, Guo Y, Peng L, Fang H, Wang Z, Zheng Y, et al. *In vivo* targeted, responsive, and synergistic cancer nanotheranostics by magnetic resonance imaging-guided synergistic high-intensity focused ultrasound ablation and chemotherapy. *ACS Appl Mater Interfaces*. (2018) 10:15428–41. doi: 10.1021/acsomega.8b01967
33. Ornelas A, Zacharias-Millward N, Menter DG, Davis JS, Lichtenberger L, Hawke D, et al. Beyond COX-1: the effects of aspirin on platelet biology and potential mechanisms of chemoprevention. *Cancer Metastasis Rev*. (2017) 36:289–303. doi: 10.1007/s10555-017-9675-z
34. Liu TS. Study on clopidogrel combined with aspirin in the treatment of acute myocardial infarction. *Med Inform*. (2020) 33:59–61.

**Conflict of Interest:** The authors declare that the research was conducted in the absence of any commercial or financial relationships that could be construed as a potential conflict of interest.

Copyright © 2021 Zhang, Liu, Chang, Hu, Teng, Li, Zhang and Chi. This is an open-access article distributed under the terms of the Creative Commons Attribution License (CC BY). The use, distribution or reproduction in other forums is permitted, provided the original author(s) and the copyright owner(s) are credited and that the original publication in this journal is cited, in accordance with accepted academic practice. No use, distribution or reproduction is permitted which does not comply with these terms.